Biosensors and Bioelectronics 189 (2021) 113374

Contents lists available at ScienceDirect

Biosensors and Bioelectronics

journal homepage: www.elsevier.com/locate/bios

Electrochemiluminescence biosensor for thrombin detection based on metal organic framework with electrochemiluminescence indicator embedded in the framework

Qingqing Huang, Fang Luo, Cuiying Lin *, Jian Wang, Bin Qiu, Zhenyu Lin **

Ministry of Education Key Laboratory for Analytical Science of Food Safety and Biology, Fujian Provincial Key Laboratory of Analysis and Detection for Food Safety, College of Chemistry, Fuzhou University, Fuzhou, Fujian, 350116, China

ARTICLE INFO

Keywords:
Metal organic frameworks
Electrochemiluminescence
Biosensors
Aptamer
$RecJ_f$ exonuclease

ABSTRACT

$Ru(dcbpy)_3^{2+}$-polyethyleneimine-L-lysine (Ru-PEI-L-lys) had been immobilized on metal organic frameworks (ZIF-8) to form an electrochemiluminescent(ECL) indicator (Ru-PEI-L-lys-ZIF-8). In this ECL indicator, PEI-L-lys is used as a co-reactant. Platinum nanoparticles (PtNPs) has been mixed with Ru-PEI-L-lys-ZIF-8 to form a thin film to increase the electron transfer rate and enhanced the ECL response of the system. The prepared material had been characterized carefully and been combined with high selectivity of aptamer to develop a ECL biosensor for thrombin detection. $RecJ_f$ exonuclease (an ssDNA specific exonuclease) assistant target recycling amplification has been adopted to enhance the sensitivity of the system. The ECL response of the system has a linear relationship with logarithm of thrombin concentration in the range of 1 fM to 10 pM with a detection limit of 0.02 aM. This work not only provides a new strategy for the design and synthesis of high performance and stable ECL indicator, but also opens up a new approach for the development of highly sensitive ECL sensors for biological analysis.

1. Introduction

Electrochemiluminescence (ECL) is a luminescent phenomenon controlled by electrochemical reaction, which has low cost, low background noise and simple operation procedure (Kwon and Myoung, 2020). It is widely used in environmental monitoring, food and clinical diagnosis. Ruthenium (II) tris (2,2-bipyridyl) ($Ru(bpy)_3^{2+}$) and its derivative have attracted considerable interest due to high luminescence, good stability and outstanding electrochemistry reversibility (Liu et al., 2017b). Materials such as Au nanoparticles (AuNPs), mesoporous silica nanoparticles (MSN), g-C_3N_4 nanosheets (g-C_3N_4 NS), carbon nanotubes have been used to load $Ru(bpy)_3^{2+}$ and acted as ECL indicators to develop ECL biosensors (Cheng et al., 2020; Gao et al., 2020; Liu et al., 2021). For example, 3,4,9,10-perylenetetracarboxylic acid with good membrane-forming property and negatively charged AuNPs were used to immobilize $Ru(bpy)_3^{2+}$, improving the stability and amplified $Ru(bpy)_3^{2+}$ ECL signal, which was successfully applied to detect concanavalin A (Wang et al., 2017). A large amount of $Ru(bpy)_3^{2+}$ was loaded into MSN and then used to develop biosensor for quantitative detection of Troponin I (Hong et al., 2020). Metal organic frameworks (MOF) are porous materials with periodic network framework formed by self-assembly metal ions and organic ligands, which have become popular loading nanomaterials (Bieniek et al., 2020; Mao et al., 2014) owing to large specific surface area, tailorable structure and high porosity and have been used to load $Ru(bpy)_3^{2+}$ to develop ECL biosensors as well. For example, a dual wavelength proportional ECL resonance energy transfer sensor was constructed with g-C_3N_4 NS and Ru@MOF (luminescent functionalized MOF, ECL indicator) as energy donor-receptor pairs (Cheng et al., 2020). An ECL immunosensor for mucin 1 detection was proposed using a novel mesoporous luminescent MOF (Ru-PCN-777) as ECL indicator (Hu et al., 2018). In these studies, the luminescent indicators were directly doped into MOF, thus the ECL probes can inevitably leak from the MOF carrier after long time storage, resulting in the relative low reproducibility. Consequently, it is necessary to find some way to improve the stability of prepared ECL indicator.

Aptamer have the advantages of easy synthesis and modification, low cost and high specificity (Riccardi et al., 2020; Yu and Wu, 2019). Thrombin is a serine protease that catalyzes the conversion of fibrinogen

* Corresponding author. Department of Chemistry, Fuzhou University, Fuzhou, Fujian, 350116, China.
** Corresponding author. Department of Chemistry, Fuzhou University, Fuzhou, Fujian, 350116, China.
E-mail addresses: lcuiying@fzu.edu.cn (C. Lin), zylin@fzu.edu.cn (Z. Lin).

https://doi.org/10.1016/j.bios.2021.113374
Received 10 March 2021; Received in revised form 8 May 2021; Accepted 21 May 2021
Available online 29 May 2021

to fibrin to facilitate blood clotting and plays a crucial role in cardiovascular disease, liver disease, Alzheimer's disease, leukemia and other blood-related diseases. Therefore, quantitative detection of thrombin is of great significance for the diagnosis, treatment and evaluation of drug efficacy of these diseases (Cheng et al., 2019; Deng et al., 2020; Liu et al., 2017a; Yan et al., 2020; Zhang et al., 2020). Many sensitive aptamers based on ECL biosensor for thrombin have been developed. However, more effort is still needed to develop simple but sensitive biosensor for thrombin detection.

In this study, Ru(dcbpy) $_3^{2+}$ with good ECL property was linked with polyethyleneimine-L-lysine(EI-L-lys)through amide bond to form a luminescent framework material (Ru-PEI-L-lys). Then amino group in luminescent skeleton and Zn^{2+} in the 2-methylimidazole zinc salt (ZIF-8) coordinated to form a luminescent material (Ru-PEI-L-lys-ZIF-8). Here, PEI-L-lys was used as a co-reactant, therefore no additional co-reactant was required. The prepared Ru-PEI-L-lys-ZIF-8 was used to construct an ECL biosensor based on $RecJ_f$ exonuclease for thrombin detection, whose principle is shown in Scheme 1. Ru-PEI-L-lys-ZIF-8 has poor conductivity, so the high conductivity of platinum nanoparticles (PtNPs) was mixed with Ru-PEI-L-lys-ZIF-8. Then, the mixture was dropped on the electrode surface to form a thin film with high ECL response. The present of PtNPs promoted electron transfer and improved ECL efficiency, which could also react with thiol of capture probe (CDNA) through Pt-S interaction. Then ferrocene (Fc) modified aptamer (Fc-aptamer) chain was hybridized with CDNA to form CDNA/Fc-aptamer duplex (dsDNA) on the electrode surface, enabling Fc close to the electrode surface. The ECL signal was quenched as Fc could inhibit the ECL luminescence of Ru(bpy) $_3^{2+}$ and its efficient derivatives (Gao et al., 2017; Jian et al., 2019). In the presence of target, the aptamer preferred to form thrombin/aptamer complex in lieu of CDNA/Fc-aptamer duplex, resulting in the disassembly of original duplex and the releasing of Fc from the electrode surface, then ECL signal of the system was enhanced. As the target concentration in organism is usually low, it is necessary to adopt signal amplification strategies to improve the sensitivity. $RecJ_f$ exonuclease (Yang et al., 2020) can catalyze the removal of 5′-3′ deoxynucleotide to selectively cut single-stranded DNA (ssDNA) (Ni et al., 2018; Wei et al., 2020). The single strand of aptamer labeled with ferrocene in form of thrombin/aptamer complex can be specifically cut with the releasing of target. Then, the thrombin can interact with the aptamer immobilized on electrode surface again and thus triggers the next cycle. By this means, signal amplification can be realized and a sensitive ECL biosensor for thrombin can be developed. The developed ECL biosensor has been applied to detect thrombin in the serum samples with satisfied results.

2. Experimental section

2.1. Materials

Tris (4, 4′-dicarboxylicacid-2, 2′-bipyridyl) ruthenium(II) dichloride (Ru(dcbpy) $_3^{2+}$) was obtained from SunaTech Inc (Suzhou, China). Polyethyleneimine (PEI), L-lysine (L-lys), 2-methylimidazole (2-MI), N-Hydroxysuccinimide (NHS), ascorbic acid (AA), 1-ethyl-3'-[3-dimethylaminopropyl]carbodiimide hydrochloride (EDC), chitosan (CS), potassium ferricyanide ($K_3[Fe(CN)_6]$), potassium ferrocyanide ($K_4[Fe(CN)_6].3H_2O$), potassium chloride (KCl), 6-mercaptohexan-1-ol (MCH), glutathione (GSH), sodium chloride (NaCl), boracic acid (H_3BO_3, Pt storage buffer), Tris-borate-EDTA(TBE) were obtained from Aladdin Chemical Reagent Co. Ltd. (Shanghai, China). Thrombin (TB), alkaline phosphatase (ALP), alpha fetal protein (AFP) and urease (UA) were purchased from Sigma-Aldrich (St. Louis, MO, USA). Methyl alcohol, ethyl alcohol, and zinc nitrate hexahydrate ($Zn(NO_3)_2.6H_2O$) were bought from Shanghai Chemical Reagent Company (Shanghai, China). $RecJ_f$ exonuclease and 10 × NE Buffer 2 (pH = 7.9 hybridization buffer, 50 mM NaCl, 10 mM Tris-HCl, 10 mM $MgCl_2$, 1 mM DTT) were purchased from New England Biolabs Ltd. (Beijing, China). Phosphate buffer solution (PBS, pH = 7.4) and oligonucleotides were obtained from Sangon Biotech Co., Ltd (Shanghai, China). All reagents used are analytically pure and used directly without further purification. Ultrapure water (Milli-Q, Millipore, resistance 18.2 MΩ cm) were used throughout the experiments.

The sequence used:

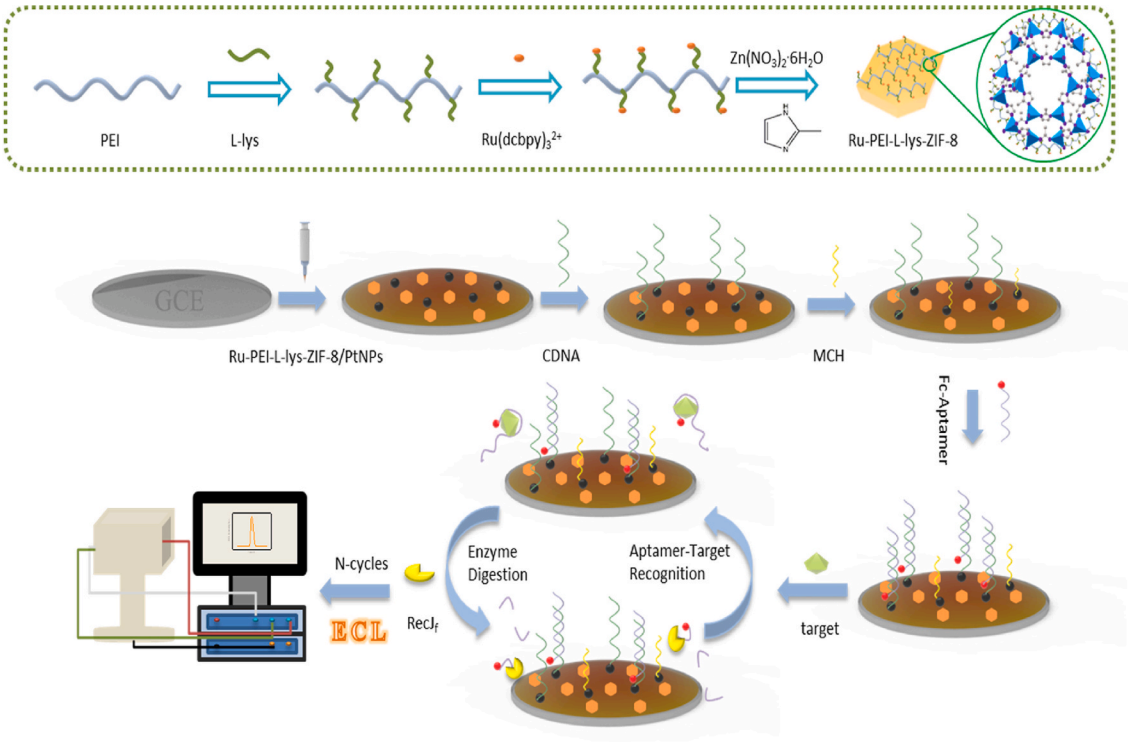

Scheme 1. Schematic illustration of the proposed ECL biosensors for thrombin detection.

Fc-aptamer: 5′-AAAGG TTGGT GTGGT TGG-Fc-3’.
CDNA: 5′-SH-C_6-CCAAC CACAC CAACC TTT-3’.

2.2. Apparatus

The ECL signals were measured with a BPCL Ultra-Weak Luminescence Analyzer (Institute of Biophysics, Chinese Academy of Science, Beijing, China). Cyclic voltammetry (CV) experiments and electrochemical impedance spectroscopy (EIS) were measured with a CHI660D electrochemical workstation (Chenhua Instruments, Shanghai, China). The voltage of photomultiplier tube (PMT) was set at −800 V. The glassy carbon electrode (GCE) (3 mm in diameter), Ag/AgCl electrode and platinum electrode were used as working, reference and counter electrodes, respectively. EIS were carried out in a mixture of 5 mM [Fe (CN)$_6$]$^{3-/4-}$ and 0.1 M KCl, with EIS frequencies ranging from 0.1 Hz to 10 kHz at the open circuit voltage of instrument. CV scanning was performed at a sweep rate of 0.1 V/S in the range of 0.4 V-1.6 V. The morphologies were characterized and energydispersive X-ray spectroscopy by a scanning electron microscope (SEM, Nova NanoSEM 230, Czech).

2.3. Polyacrylamide gel electrophoresis analysis

Polyacrylamide gel electrophoresis (12%, PAGE) was conducted to verify the feasibility of proposed strategy. The project was performed in 0.5 × TBE buffer (pH = 8.4) at a constant voltage of 80 V for 120 min at room temperature.

2.4. Synthesis of Ru-PEI-L-lys-ZIF-8

Firstly, 2-MI (5 mL, 20 mM) and Zn $(NO_3)_2.6H_2O$ (5 mL, 20 mM) were continuously stirred at room temperature for 6 h to synthesize ZIF-8. Secondly, L-lys (1.46 mg) was dissolved in ultrapure water (1 mL), then EDC (76.75 mg) and NHS (11.5 mg) were added, and the solution was evenly mixed after shaking for 20 min. Thirdly, PEI (1 mL, 1%, w/w) was added to the above solution and reacted for 1 h under magnetic stirring to synthesize the PEI-L-lys framework. Fourthly, Ru(dcbpy)$_3$Cl$_2$ (9 mg) was dissolved in ultrapure water (1 mL), EDC (30.7 mg) and NHS (4.6 mg) were added, and then PEI-L-lys was added to enable the solution evenly mixed after shaking for 20 min, and then the Ru-PEI-L-lys skeleton was obtained by reaction for 1 h. Finally, ZIF-8 solution (10 mL) and Ru-PEI-L-lys solution (3 mL) were mixed uniformly and left overnight to obtain Ru-PEI-L-lys-ZIF-8. The obtained solution was centrifuged and washed three times and dispersed in 10 mL of ultrapure aqueous solution for later use.

2.5. Synthesis of PtNPs

PtNPs were synthesized according to the method reported earlier (Huang et al., 2019). Chloroplatinic acid (5 mL, 1 mM) was heated at 80 °C and 600 r/min for 20 min. AA (500 μL, 0.4 M) was added and the reaction was continued at 80 °C for 30 min. After being cooled to room temperature, the mixture was centrifuged and washed three times, PtNPs was resuspension in Pt storage buffer (5 mL) and store in a refrigerator at 4 °C for later use.

2.6. Preparation of biosensors

The surface of GCE was polished with 0.3 μm and 0.05 μm Al_2O_3 polishing powders (0.3 μm and 0.05 μm) and rinsed with ultrapure water firstly. Ru-PEI-L-lys-ZIF-8 (10 μL, 0.8 mg/mL), PtNPs (25 μL, 0.23 mg/mL) and CS (1.1 μL, 0.5%, w/w) were mixed to obtain Ru-PEI-L-lys-ZIF-8/PtNPs dispersion. Ru-PEI-L-lys-ZIF-8/PtNPs (10 μL) was dropped on the surface of pretreated GCE and dried naturally to obtain the Ru-PEI-L-lys-ZIF-8/PtNPs/GCE luminous substrate. CDNA (10 μL, 1 μM) was dropped and incubated in dark for 3 h, and the capture probe was fixed on the surface of GCE through Pt–S bond self-assembly. Subsequently, MCH (10 μL, 1 mM) was added and reacted for 30 min in the dark to block nonspecific recognition sites. After the above treatment, Fc-aptamer (10 μL) was added to the modified glassy carbon electrode to react for 90 min. After each step of modification, the electrodes were washed with ultrapure water and dried with nitrogen.

Different concentration of thrombin (10 μL) and RecJ_f exonuclease (0.3 U/μL) were dropped on the surface of GCE and reacted for 40 min. The biosensor was washed with ultrapure water and dried with nitrogen. Such ECL biosensor was prepared at 37 °C.

3. Results and discussion

3.1. Characterization of Ru-PEI-L-lys-ZIF-8

The functional groups on the Ru-PEI-L-lys-ZIF-8 and original materials were compared via FT-IR characterization (Fig. 1). Structural dipyridyl groups (770 cm^{-1} and 725 cm^{-1}) in Ru(dcbpy)$_3^{2+}$, N-H bending vibration (1640cm^{-1}) in PEI-L-lys, C═N stretching vibration (1580 cm^{-1}) and C-N stretching vibration (1150 cm^{-1} and 993 cm^{-1}) in ZIF-8 can clearly observed in the FT-IR spectrum of Ru-PEI-L-lys-ZIF-8. The characterization results verify successful immobilization of Ru (dcbpy)$_3^{2+}$, PEI-L-lys into the ZIF-8.

Fig. 2A and B shows the UV absorption spectrum and fluorescence spectrum of synthesized Ru-PEI-L-lys-ZIF-8. The absorption peak of 483 nm appeared in the UV absorption spectrum which can be attributed to the charge transfer of π(Ru)→π*(dcbpy). The slight blue shift of UV spectrum at 16 nm can be attributed to the formation of amide bonds, indicating the interaction of Ru(dcbpy)$_3^{2+}$ and PEI-L-lys. While at the maximum excitation wavelength of 480 nm, the strongest emission peak of Ru(dcbpy)$_3^{2+}$ was red shifted from 644 to 654 nm, which indicates that some Ru(dcbpy)$_3^{2+}$ is distributed inside ZIF-8 since some photons in the Ru-PEI-L-lys-ZIF-8 have undergone an energy transfer process.

SEM was used to characterize the morphology of ZIF-8, Ru-PEI-L-lys-ZIF-8 and Ru-PEI-L-lys-ZIF-8/PtNPs. Fig. 2C and Fig. S1A in supporting information (SI) were the SEM images of ZIF-8, displaying regular dodecahedral structure with the size of 420 ± 20 nm. As shown in Fig. 2D and Fig. S1B, Ru-PEI-L-lys-ZIF-8 was uniformly wrapped by membranous substance. The edge became a little blurred, but the structure remained when the Ru-PEI-L-lys luminescent framework was doped. From Fig. 2E and Fig. S1C, PtNPs were well distributed on the surface of the material. The EDS spectrum in SEM (Fig. 2F and

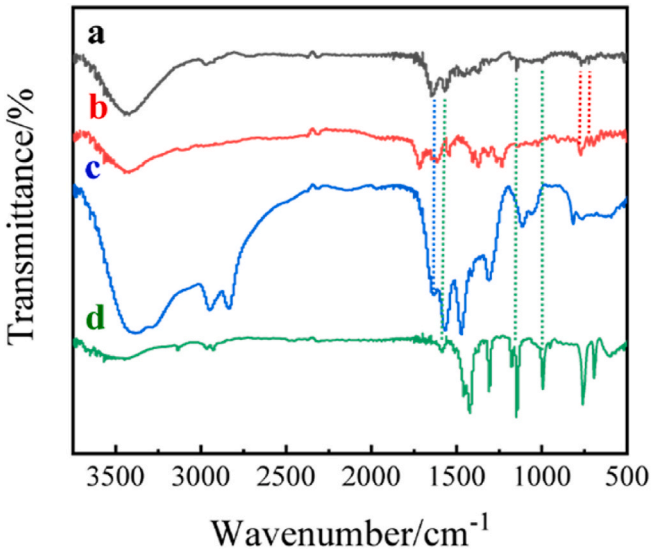

Fig. 1. FT-IR characterization of (a) Ru-PEI-L-lys-ZIF-8, (b) Ru(dcbpy)$_3^{2+}$, (c) PEI-L-lys and (d) ZIF-8.

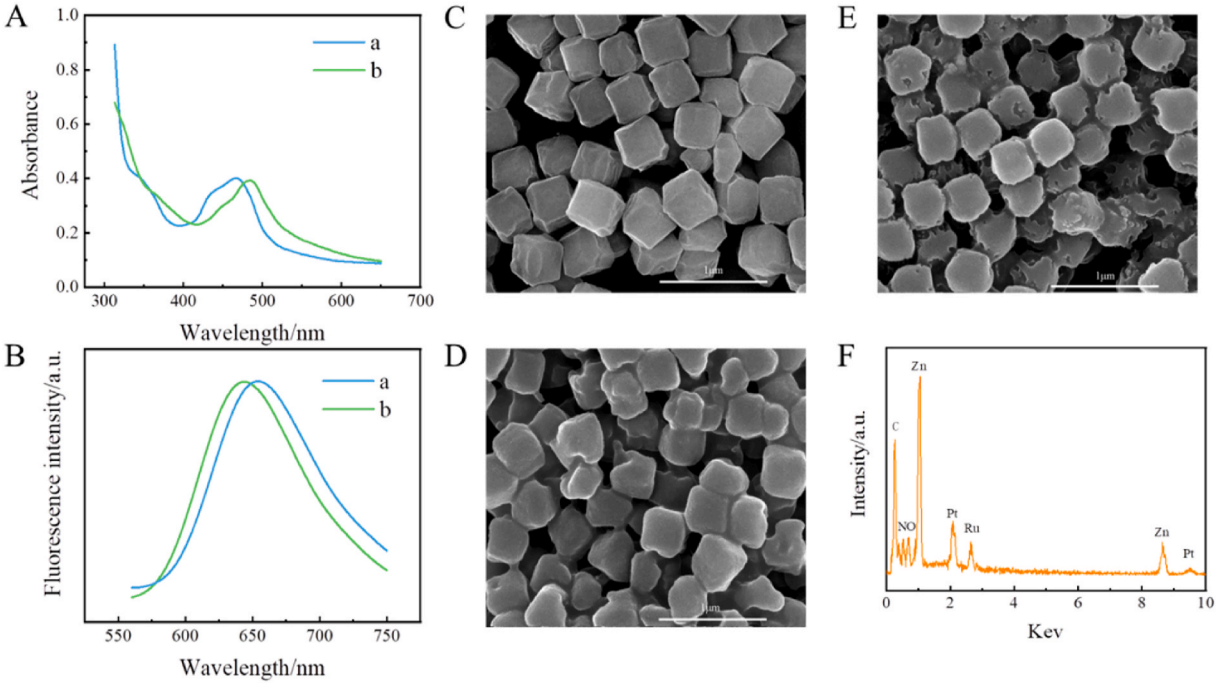

Fig. 2. (A) UV–vis absorption spectra of (a) Ru-PEI-L-lys-ZIF-8 and (b) $Ru(dcbpy)_3^{2+}$, (B) Fluorescence emission spectra of (a) Ru-PEI-L-lys-ZIF-8 and (b)$Ru(dcbpy)_3^{2+}$. SEM images of (C) ZIF-8, (D) Ru-PEI-L-lys-ZIF-8, (E) Ru-PEI-L-lys-ZIF-8/PtNPs and (F) EDS of Ru-PEI-L-lys-ZIF-8/PtNPs.

Figs. S1D–F) revealed that Zn, Ru, N, Pt were distributed in the synthesized Ru-PEI-L-lys-ZIF-8/PtNPs nanoparticles.

3.2. ECL character of Ru-PEI-L-lys-ZIF-8 and potential mechanical

CV and ECL potential curves in PBS (0.1 M, pH = 7.4) were tested. As shown in Fig. 3A, the current signal started at about 1.10 V and reached

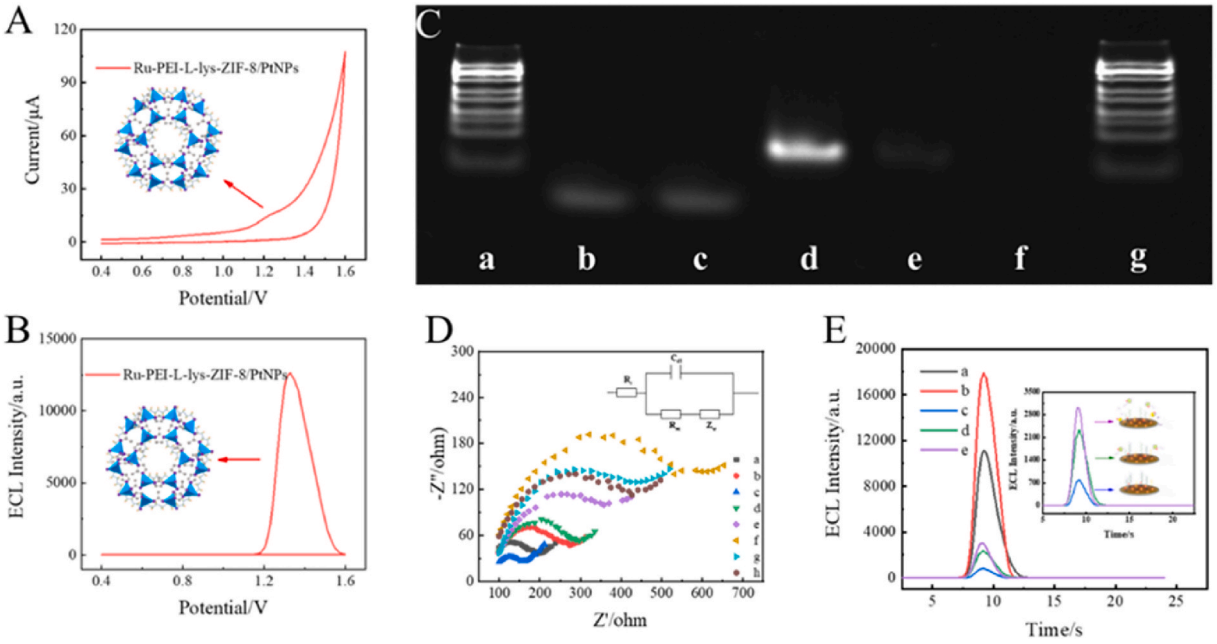

Fig. 3. (A) CV and (B) ECL potential curves of Ru-PEI-L-lys-ZIF-8/PtNPs. (C) 12% Gel electrophoresis image of (lane a and g) Marker, (lane b) CDNA (20 μM), (lane c) Fc-aptamer (20 μM), (lane d) CDNA (5.0 μM) mixed with Fc-aptamer (5.0 μM), (lane e) CDNA (5.0 μM) mixed with Fc-aptamer (5.0 μM) and thrombin, (lane f) CDNA (5.0 μM), Fc-aptamer (5.0 μM) mixed with $RecJ_f$ exonuclease and thrombin. (D) EIS characterization of the stepwise modification of electrodes: (a) GCE, (b) Ru-PEI-L-lys-ZIF-8/GCE, (c) Ru-PEI-L-lys-ZIF-8/PtNPs/GCE, (d) CDNARu-PEI- L-lys-ZIF-8/PtNPs/GCE, (e) MCH/CDNA/Ru-PEI-L-lys-ZIF-8/PtNPs/GCE, (f)Fc-aptamer/MCH/CDNA/Ru-PEI-L-lys-ZIF-8/PtNPs/GCE, (g)thrombin/Fc-aptamer/MCH/CDNA/Ru-PEI-L-lys-ZIF-8/PtNPs/GCE, (h)thrombin/$RecJ_f$ exonuclease/Fc-aptamer/MCH/CDNA/Ru-PEI-L-lys-ZIF-8/PtNPs/GCE. (E) ECL signals of different modified electrodes in 0.10 M PBS (PH = 7.4) (a)Ru-PEI-L-lys-ZIF-8, (b) Ru-PEI-L-lys-ZIF-8/PtNPs, (c) Fc-aptamer /MCH/CDNA/Ru-PEI-L-lys-ZIF-8/PtNPs/GCE, (d) thrombin/Fc-aptamer /MCH/CDNA/Ru-PEI-L-lys-ZIF-8/PtNPs/GCE, (e) thrombin/$RecJ_f$ exonuclease /Fc-aptamer/MCH/CDNA/ Ru-PEI-L-lys-ZI8/PtNPs/GCE. The concentration of thrombin and $RecJ_f$ exonuclease were 5×10^{-11} M and 0.3 U/μL, reaction time of $RecJ_f$ exonuclease was 40 min.

the maximum at 1.25 V, which is consistent with the oxidation potential of $Ru(dcbpy)_3^{2+}$ (Ye et al., 2019). The high ECL signal produced by Ru-PEI-L-lys-ZIF-8 is shown in Fig. 3B, which indicates that $Ru(dcbpy)_3^{2+}$ in Ru-PEI-L-lys-ZIF-8 nanomaterials still maintains its ECL characteristics.

The possible ECL mechanisms of Ru-PEI-L-lys-ZIF-8 were outlined as follows according to previous literature (Carrara et al., 2017). The luminous specie, Ru(II)*-PEI-L-lys-ZIF-8, was produced by the intramolecular electron transport between PEI-L-lys· and Ru (II)-PEI-L-lys··ZIF-8. In detail, both Ru(III) and PEI-L-lys are oxidized to form Ru(III) and PEI-L-lys·$^+$, where PEI-L-lys·$^+$ is rapidly protonated to form intermediate PEI-L-lys·. PEI-L-lys· interacts with Ru(III) to form excited state Ru(II)*, and finally produces light signal in the process of transition back to ground state.

$$Ru(II)\text{-}PEI\text{-}L\text{-}lys\text{-}ZIF\text{-}8\text{-}2e^- \rightarrow Ru(III)\text{-}PEI\text{-}L\text{-}lys\cdot^+\text{-}ZIF\text{-}8$$

$$Ru(III)\text{-}PEI\text{-}L\text{-}lys\cdot^+\text{-}ZIF\text{-}8 \rightarrow Ru(III)\text{-}PEI\text{-}L\text{-}lys\cdot\cdot\text{ZIF}\text{-}8+H^+$$

$$Ru(III)\text{-}PEI\text{-}L\text{-}lys\cdot\cdot\text{ZIF}\text{-}8 \rightarrow Ru(II)^*\text{-}PEI\text{-}L\text{-}lys\text{-}ZIF\text{-}8$$

$$Ru(II)^*\text{-}PEI\text{-}L\text{-}lys\text{-}ZIF\text{-}8 \rightarrow Ru(II)\text{-}PEI\text{-}L\text{-}lys\text{-}ZIF\text{-}8+hv$$

3.3. Feasibility of the proposed biosensor for thrombin detection

Polyacrylamide gel electrophoresis was performed to verify that the target can reduce CDNA/Fc-aptamer duplex. It demonstrated the vital role of $RecJ_f$ exonuclease in signal amplification. As shown in Fig. 3C, lane a and lane g represented the bands of marker, lane b and lane c were CDNA and the Fc-aptamer chain, respectively. Lane d was the band of CDNA/Fc-aptamer duplex. Lane e was band with duplex and the target substance. The number of dsDNA decreased and the bands became shallower due to the specific binding of thrombin/aptamer complex, which indicates the importance of target in this assay. Lane f was the channel where dsDNA, the target substance and $RecJ_f$ exonuclease were added, whose bands were disappeared. This fact suggests that the exonuclease cleavage reaction of the ssDNA occurs under target assisted conformation switch. Electrochemical impedance spectroscopy (EIS) is an effective method to characterize the surface of electrodes using redox probes. The semicircle observed at higher frequencies corresponds to the charge transfer limited process, and the increase in the semicircle diameter reflects the increase in the resistance of interface to charge transfer. In Fig. 3D, the bare GCE showed a small Ret (curve a), the resistance obtained at the Ru-PEI-L-lys-ZIF-8/PtNPs modified electrode (curve c) obviously decreased compared with that obtained at the Ru-PEI-L-lys-ZIF-8 (curve b) due to the excellent conductivity of PtNPs, which facilitated electron transfer. After that, the Ret kept increasing when CDNA (curve d), MCH (curve e), Fc-aptamer (curve f) were continuously modified onto the electrode. The gradual increasing of impedance values is due to the fact that the negatively charged DNA and MCH hinder the electron transfer of $[Fe(CN)_6]^{3-/4-}$ reaching the electrode surface. When the target was added to electrode surface and incubated, the impedance decreased (curve g). The reason lies in that thrombin competes with the CDNA to form a thrombin/Fc-aptamer complex, leading to a decreased electron transfer resistance. The addition of $RecJ_f$ exonuclease can cut the DNA into fragments along the 5′-3′ direction of the ssDNA, thereby exposing the target to trigger next cycling. After multiple cycles, the decrease of dsDNA leads to the decrease of negative charge on GCE surface, and finally leads to the significant decrease of impedance (curve h). The ECL signals at different stage were tested. As shown in Fig. 3E, we compared the ECL intensities of Ru-PEI-L-lys-ZIF-8 (lane a) and Ru-PEI-L-lys-ZIF-8/PtNPs (lane b) under the same condition. The results showed that the ECL signal increased from 11114 a.u. to 17926 a.u. after the addition of PtNPs, which implies that PtNPs promote the transfer of electrons to increase the ECL signal. It was confirmed that the addition of target and $RecJ_f$ exonuclease would increase the ECL intensity. Line c was the ECL signal after the modification of Fc-aptamer, whose reason lies in the quench of ECL of Ru-PEI-L-lys-ZIF-8/PtNPs by Fc. As Fc quenched ECL of Ru-PEI-L-lys-ZIF-8/PtNPs, the ECL response decreased, resulting in the ECL biosensor in the off state (signal value of 800 arbitrary units). Line d showed that the signal was restored, which demonstrates that the target can be combined with the aptamer to keep the ferrocene away from the electrode surface and hence the ECL biosensor is turned on. As shown in lane e, the signal recovery was enhanced, indicating that exonuclease cuts single chain and releases the target. To conclude, the above results show the feasibility of our scheme.

3.4. Optimization of the experimental conditions

To obtain the best detection performance, the Fc-aptamer concentration and incubation time, $RecJ_f$ exonuclease concentration and digestion time were optimized. Fc can quench the ECL signal of Ru-PEI-L-lys-ZIF-8, the amount of Fc-aptamer affects the performance of the proposed biosensor greatly. As shown in Fig. 4A, the ECL intensity gradually decreased as the concentration of Fc-aptamer shifted from 0.25 to 1.25 μM, demonstrating the effectiveness of Fc in inhibiting ECL. When the concentration of Fc-aptamer increased to 1.25 μM, the ECL intensity reached a plateau, therefore 1.25 μM was selected as the optimal reaction concentration. The concentration of $RecJ_f$ exonuclease was optimized for the reason that exonuclease amplifies the ECL signal in the system. The ECL value gradually increased with the concentration of $RecJ_f$ exonuclease from 0.2 to 0.4 U/μL, and then became stable when the concentration value exceeded 0.4 U/μL (Fig. 4A). Therefore, 0.4 U/μL of $RecJ_f$ exonuclease was used for the following work. The effect of the time of interaction between Fc-aptamer and CDNA was optimized (Fig. 4B). ECL intensity was negatively correlated to binding time from 30 to 90 min and then converged. Therefore, the optimum incubation time of CDNA/Fc-aptamer duplex was selected at 90 min. Finally, the digestion time after adding the $RecJ_f$ exonuclease was optimized (Fig. 4B). When the digestion time of exonuclease ranged from 10 to 110 min, the ECL signal increased firstly and then became stable after 70 min. Therefore, 70 min was selected as the best condition.

3.5. Performance of the proposed biosensor

Under the optimal conditions, the relationship between the concentration of thrombin and the ECL response was studied. As shown in Fig. 5A, the system ECL increased with the enhanced target concentration. There was a good linear relationship between ECL intensity and the logarithm of thrombin concentration in the range of 1 fM to 10 pM (Fig. 5B). The linear regression equation was:

$$I_{ECL} = 1416.27 \lg C_{TB} + 24435.85$$

Here, C_{TB} is the concentration of thrombin (given in units of M), and the correlation coefficient (R^2) is 0.9918. The limit of detection (LOD) of the sensor was 0.02 aM (S/N = 3). Table S1 shows the comparison results of this work with other reported analytical methods. Compared with previous reports, the proposed biosensor shows a better LOD and linear range.

To evaluate the selectivity of proposed biosensor, bovine serum albumin (BSA), alkaline phosphatase (ALP), alpha-fetoprotein (AFP), urease (UA), glutathione (GSH), potassium ion (K^+) and sodium ions (Na^+) were selected as the model interfering substances. The concentration of thrombin was 50 fM, while the concentration of interferences was 10 pM. As shown in Fig. 5C, the detection results of interfering substance in the serum were similar to those in blank test. However, the present of thrombin caused more ECL changing. When the mixture of thrombin, BSA, ALP, AFP, UA, GSH, K^+, Na^+ added together, the ECL response decreased by 5.6% compared with that of single thrombin. All

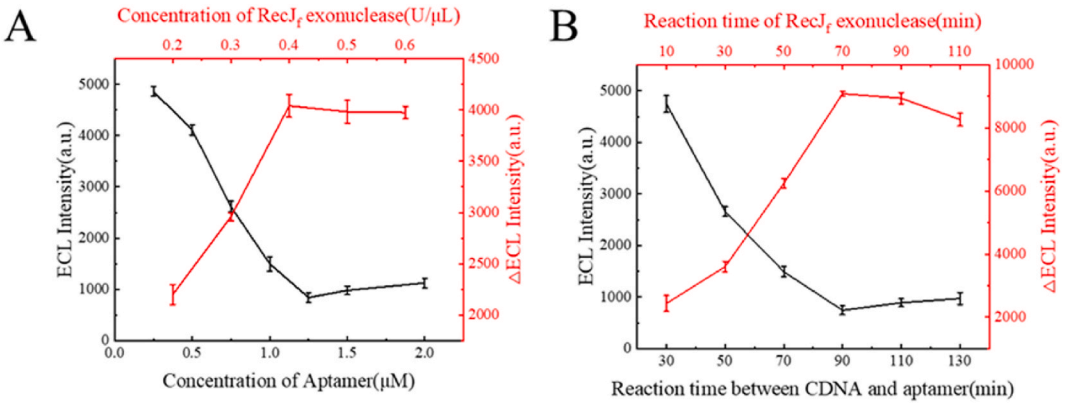

Fig. 4. (A)Effect of concentration of Fc-aptamer on the ECL intensity and effect of concentration of $RecJ_f$ exonuclease on the ECL intensity, (B) Effect of reaction time between CDNA and Fc-aptamer on the ECL intensity and effect of the target and exonuclease digesting time on the ECL intensity.

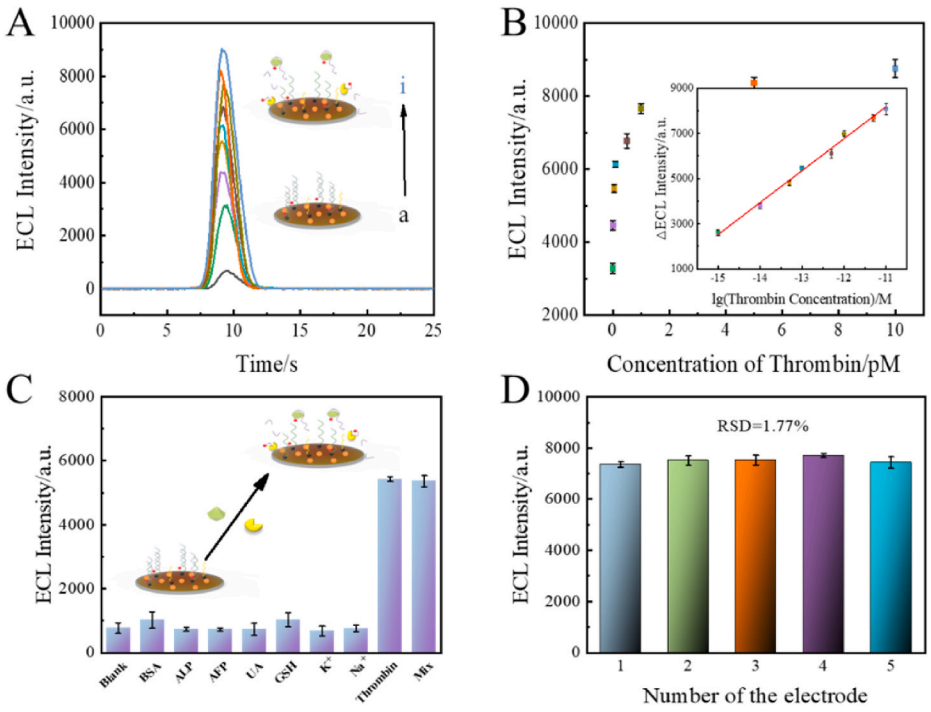

Fig. 5. (A)ECL response at concentrations of thrombin. (a) 0 M, (b) 0.001 pM, (c)0.01 pM, (d) 0.05 pM, (e) 0.1 pM, (f) 0.5 pM, (g) 1 pM, (h) 5 pM, (i) 10 pM, (B) Linear relationship between the ECL and thrombin concentration. (C) Selectivity of the biosensor with different interferences, (D) Repeatability of thrombin detection by 5 parallel measurements (RSD = 1.77%), thrombin concentration was 1 pM. Error bars = SD, (n = 3).

of the above outcomes verify that the biosensor has good selectivity.

Five different electrodes were used to construct and evaluate the sensor, and the relative standard deviation (RSD) was 1.77%, indicating that the proposed ECL sensor has outstanding reproducibility (Fig. 5D).

The recovery assay can be used to evaluate the applicability of the developed biosensors. As shown in Table S2, the recovery rate was between 97.8% and 103.8%, indicating that the proposed ECL biosensor has great potential for the detection of thrombin content in real biological samples.

4. Conclusion

In summary, we successfully prepared Ru-PEI-L-lys-ZIF-8 luminescent composite indicator through a simple synthesis method. Compared with ECL biosensors constructed by traditional composite materials that require doping of luminescent reagents in a solid matrix, the proposed luminescent indicator has a significant advantage of not easy to leak. In addition, using the aptamer recognition element with quencher and $RecJ_f$ exonuclease as a signal amplification strategy, a highly sensitive ECL biosensor was designed for the sensitive and selective detection of thrombin in serum. Besides, PtNPs is used in the construction of the biosensor, which can not only connect with SH-labeled DNA, but also improve the efficiency of electron transfer. The detection limit of the ECL biosensor is as low as 0.02 aM, and the linear range is 1 fM to 10 pM. Furthermore, the proposed strategy also has high specificity, accuracy and good recovery rate in serum samples. The proposed ECL platform can replace thrombin aptamers by changing specific aptamers, and has huge potential applications in the development of various sensitive aptamer sensors for detecting other disease-related proteins. Therefore, the ECL biosensor based on MOF provides a new measurement scheme for the ultra-sensitive detection of biomarkers, which is of great significance in early clinical disease diagnosis and bioanalysis.

CRediT authorship contribution statement

Qingqing Huang: Conceptualization, Methodology, Validation, Formal analysis, Investigation, Data curation, Writing – original draft. **Fang Luo:** Conceptualization, Methodology, Investigation, Data curation, Writing – original draft, Visualization. **Cuiying Lin:** Writing – review & editing, Funding acquisition. **Jian Wang:** Supervision. **Bin Qiu:** Supervision. **Zhenyu Lin:** Conceptualization, Methodology, Funding acquisition, Writing – review & editing.

Declaration of competing interest

The authors declare that they have no known competing financial interests or personal relationships that could have appeared to influence the work reported in this paper.

Acknowledgments

This project was financially supported by National Sciences Foundation of China (21775026,21974020), the cooperative project of production and study in University of Fujian Province (2018Y4007), the Sciences Foundation of Fujian Province (2018J01685, 2018J01682), STS Key Project of Fujian Province (2017T3007) and the United Fujian Provincial Health and Education Project for Tackling the Key Research P. R. China (2019-WJ-11).

Appendix A. Supplementary data

Supplementary data to this article can be found online at https://doi.org/10.1016/j.bios.2021.113374.

References

Bieniek, A., Terzyk, A.P., Wiśniewski, M., Roszek, K., Kowalczyk, P., Sarkisov, L., Keskin, S., Kaneko, K., 2020. Prog. mater. sic, 100743.
Carrara, S., Arcudi, F., Prato, M., DeCola, L., 2017. Angew. Chem. Int. Ed. 56 (17), 4757–4761.
Cheng, S., Zhang, H., Huang, J., Xu, R., Sun, X., Guo, Y., 2020. Sci. Total Environ. 737, 139785.
Cheng, T., Li, X., Huang, P., Wang, H., Wang, M., Yang, W., 2019. Microchim. Acta 186, 94.
Deng, X., Wu, S., Li, Z., Zhao, Y., Duan, C., 2020. Anal. Chem. 92 (24), 15908–15915.
Gao, H., Wang, X., Li, M., Qi, H., Gao, Q., Zhang, C., 2017. Biosens. Bioelectron. 98, 62–67.
Gao, W., Liu, Y., Zhang, H., Wang, Z., 2020. ACS Sens. 5 (4), 1216–1222.
Hong, D., Jo, E.-J., Kim, K., Song, M.-B., Kim, M.-G., 2020. Small 16 (44), 2004535.
Hu, G.-B., Xiong, C.-Y., Liang, W.-B., Zeng, X.-S., Xu, H.-L., Yang, Y., Yao, L.-Y., Yuan, R., Xiao, D.-R., 2018. ACS Appl. Mater. Interfaces 10 (18), 15913–15919.
Huang, Y., Lin, C., Luo, F., Qiu, B., Guo, L., Lin, Z., Chen, G., 2019. ACS Sens. 4 (9), 2465–2470.
Jian, Y., Wang, H., Sun, X., Zhang, L., Cui, K., Ge, S., Yu, J., 2019. Talanta 199, 485–490.
Kwon, D.-K., Myoung, J.-M., 2020. ACS Nano 14 (7), 8716–8723.
Liu, M., Li, J., Li, B., 2017a. Talanta 175, 224–228.
Liu, X., Wang, Q., Chen, J., Chen, X., Yang, W., 2021. Talanta 221, 121379.
Liu, Z., Zhang, X., Cui, L., Wang, K., Zhan, H., 2017b. Sens. Actuators, B 248, 402–410.
Mao, Y., Li, J., Cao, W., Ying, Y., Hu, P., Liu, Y., Sun, L., Wang, H., Jin, C., Peng, X., 2014. Nat. Commun. 5 (1), 5532.
Ni, J., Yang, W., Wang, Q., Luo, F., Guo, L., Qiu, B., Lin, Z., Yang, H., 2018. Biosens. Bioelectron. 105, 182–187.
Riccardi, C., Napolitano, E., Platella, C., Musumeci, D., Montesarchio, D., 2020. Pharmacol. Ther., 107649
Wang, B., Zhong, X., Chai, Y., Yuan, R., 2017. Sens. Actuators, B 245, 247–255.
Wei, M., Zhang, W., Yue, S., Yang, X., 2020. Sens. Actuators, B 312, 128019.
Yan, Y., Qiao, Z., Hai, X., Song, W., Bi, S., 2020. Biosens. Bioelectron., 112827
Yang, X., Zhao, C., Zhang, C., Wen, K., Zhu, Y., 2020. Sens. Actuators, B 323, 128666.
Ye, J., Liu, G., Yan, M., Zhu, Q., Zhu, L., Huang, J., Yang, X., 2019. Anal. Chem. 91 (20), 13237–13243.
Yu, N., Wu, J., 2019. Biosens. Bioelectron. 146, 111726.
Zhang, Q., Fan, G., Chen, W., Liu, Q., Zhang, X., Zhang, X., Liu, Q., 2020. Biosens. Bioelectron. 150, 111846.